ACS NANO

www.acsnano.org

The Schottky–Mott Rule Expanded for Two-Dimensional Semiconductors: Influence of Substrate Dielectric Screening

Soohyung Park,* Thorsten Schultz, Dongguen Shin, Niklas Mutz, Areej Aljarb, Hee Seong Kang, Chul-Ho Lee, Lain-Jong Li, Xiaomin Xu, Vincent Tung, Emil J. W. List-Kratochvil, Sylke Blumstengel, Patrick Amsalem, and Norbert Koch*

Cite This: ACS Nano 2021, 15, 14794–14803

Read Online

ACCESS | Metrics & More | Article Recommendations | Supporting Information

ABSTRACT: A comprehensive understanding of the energy level alignment mechanisms between two-dimensional (2D) semiconductors and electrodes is currently lacking, but it is a prerequisite for tailoring the interface electronic properties to the requirements of device applications. Here, we use angle-resolved direct and inverse photoelectron spectroscopy to unravel the key factors that determine the level alignment at interfaces between a monolayer of the prototypical 2D semiconductor MoS_2 and conductor, semiconductor, and insulator substrates. For substrate work function (Φ_{sub}) values below 4.5 eV we find that Fermi level pinning occurs, involving electron transfer to native MoS_2 gap states below the conduction band. For Φ_{sub} above 4.5 eV, vacuum level alignment prevails but the charge injection barriers do not strictly follow the changes of Φ_{sub} as expected from the Schottky-Mott rule. Notably, even the trends of the injection barriers for holes and electrons are different. This is caused by the band gap renormalization of monolayer MoS_2 by dielectric screening, which depends on the dielectric constant (ε_r) of the substrate. Based on these observations, we introduce an expanded Schottky-Mott rule that accounts for band gap renormalization by ε_r -dependent screening and show that it can accurately predict charge injection barriers for monolayer MoS_2. It is proposed that the formalism of the expanded Schottky-Mott rule should be universally applicable for 2D semiconductors, provided that material-specific experimental benchmark data are available.

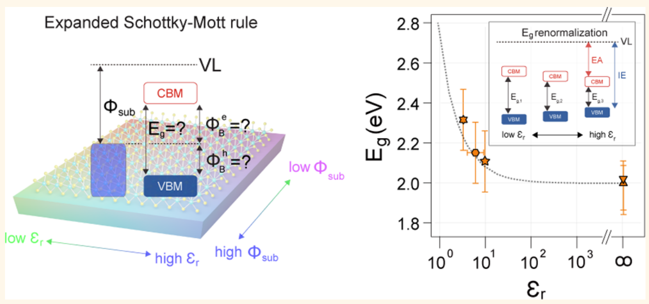

KEYWORDS: MoS_2 monolayer, 2D semiconductors, ionization energy, electron affinity, photoelectron spectroscopy, Fermi level pinning

Two-dimensional (2D) transition metal dichalcogenides (TMDCs) are intensively studied toward beyond-silicon semiconductor platforms for nanoelectronic applications because of their excellent optoelectronic properties.[1−7] Among them, monolayer (ML) molybdenum disulfide (MoS_2) has been considered for a wide range of potential applications, such as thin-film transistors (TFTs),[8−11] lateral heterojunction diodes,[12] photovoltaics,[13,14] and photodetectors.[15−17] Currently, one of the most critical issues in ML-MoS_2 based applications is the high electrical contact resistance at the ML-MoS_2/electrode junction, the reduction of which will be a key step toward high-performance devices.[18] According to the Schottky−Mott rule,[19−22] the contact resistance depends on the Schottky barrier height (SBH), which—in the simplest approximation that does not consider material-specific physicochemical interfacial interactions—is obtained as the energy difference between the electrode work function (Φ_{elec}) and the electron affinity of the conduction band minimum (CBM) or the ionization energy of the valence band maximum (VBM) of the semiconductor (see Figure 1a, where Φ_B^e and Φ_B^h are the SBH for electron and hole injection, respectively). Thus, in principle, the SBH should be tunable by varying Φ_{elec}, also for ML-MoS_2. However, Φ_B^e for ML-MoS_2 has been reported by Das et al. to be in the range of only 0.2−0.5 eV, without significant change for different Φ_{elec}.[23−26] This was attributed to Fermi level (E_F) pinning at gap states. The exact origin of E_F-pinning and a reliable approach to achieve

Received: June 6, 2021
Accepted: August 3, 2021
Published: August 11, 2021

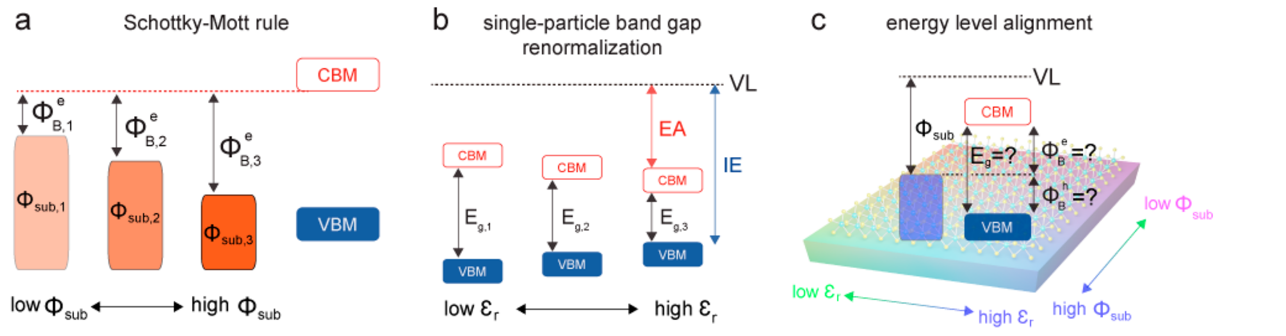

Figure 1. Illustration of the Schottky-Mott rule, single-particle band gap (E_g) renormalization, and energy level alignment for two-dimensional transition metal dichalcogenides (2D TMDCs). (a) Schematic illustration of changes in the Schottky barrier height for electrons (Φ_B^e) by varying the work function of the substrate (Φ_{sub}), and (b) band gap (E_g) renormalization by the static dielectric constant (ε_r) of the surrounding environment. VL is the vacuum level. (c) Challenges in predicting the energy level alignment at 2D TMDCs/substrate interfaces due to numerous varying parameters, such as ε_r, Φ_{sub}, or ground state charge transfer.

Ohmic contacts are still controversial issues in literature (*vide infra*) that need to be elucidated.

The pinning factor S (sometimes referred to as slope parameter) is used to characterize the strength of E_F-pinning and is defined by

$$S = \Delta\Phi_B^e/\Delta\Phi_{elec} \text{ or } S = \Delta\Phi_B^h/\Delta\Phi_{elec}$$

where $\Delta\Phi_B^e$ and $\Delta\Phi_B^h$ are changes of the SBH for electrons and holes, respectively, for a given change of the electrode work function $\Delta\Phi_{elec}$. Consequently, small S values correspond to strong E_F-pinning. On the other hand, S close to 1 corresponds to a situation where vacuum level alignment occurs, that is, the simple Schottky-Mott rule holds. So far, most studies reported S values for ML-MoS_2 in the range of 0.02−0.3, and the corresponding strong E_F-pinning is widely believed to stem from ground state charge transfer to/from sulfur vacancy−induced gap states.[24,25,27,28] In contrast, two reports recently demonstrated tunable SBHs with negligible E_F-pinning (S = 0.96), suggesting the validity of the Schottky−Mott limit, by using electrodes transferred onto the TMDC in their TFT devices.[29,30] They concluded that the reason for strong E_F-pinning in previous studies was the considerable defect creation in ML-MoS_2 that occurs during evaporation of metal electrodes onto the ML, such as chemical bond or strain formation.

It should be noted that the aforementioned Φ_B^e values were obtained via the Richardson−Dushman equation[31] ($I_{ds} = AT^2e^{-\Phi_B^e/kT}$, where I_{ds}, A, T, and k are the source-drain current, Richardson constant, absolute temperature, and Boltzmann constant, respectively) or estimated from work function measurements; direct determination of SBH values from photoemission measurements is rarely reported. However, the original Richardson−Dushman equation was derived for electron emission into vacuum, and work function measurements can be influenced by interface dipoles. Therefore, these approaches might have over- or underestimated the SBH. Furthermore, tabulated Φ_{elec} values of the respective materials were used in the estimation of Φ_B^e instead of actually measured ones, even though it is known that Φ_{elec} is highly sensitive to the electrode preparation conditions, inevitable air exposure, and surface cleaning procedures during the sample fabrication process.[32−34]

Recently, alternative electrodes, such as graphene, 1T-MoS_2, MoO_3/metal, and h-BN/metal have been proposed as superior electric contacts, some of which exhibit a lower static relative dielectric constant (ε_r), compared to the ε_r approaching infinity for conventional metals.[35] This is another important aspect because dielectric screening by the surrounding medium leads to a pronounced renormalization of the electronic structure of ML-TMDCs, including the single-particle bandgap (E_g), electron affinity (EA), and ionization energy (IE),[36−39] which is expected to also impact the SBH, as schematically shown in Figure 1b,c. A pronounced renormalization of E_g was demonstrated by a combination of angle-resolved photoelectron spectroscopy (ARPES) and angle-resolved inverse photoelectron spectroscopy (ARIPES) measurements for ML-MoS_2 on substrates with high and low ε_r.[40] From earlier optical measurements by Chernikov et al. and Lin et al., ε_r-dependent energy level renormalization was evidenced through a variation of the exciton binding energy.[41−43] Consequently, the dielectric environment, which has been largely ignored in the discussion of the SBH so far, must also be considered to reliably estimate the SBH for ML-TMDCs. The traditional Schottky−Mott rule does not consider the impact of the dielectric environment, because it is not obviously relevant for conventional 3D semiconductors, for which the rule was developed.[21] Consequently, the consideration of Φ_{sub} and ε_r in an appropriately modified Schottky-Mott rule is essential to possibly predict the SBH in 2D TMDCs, accurately and reliably.

In this contribution, we investigate the impact of Φ_{sub} and ε_r on the SBH of a ML-MoS_2 by measuring the work function, IE, and EA of ML-MoS_2 on a variety of supporting substrates by a combination of ARPES and ARIPES. We observe a substantial electronic structure renormalization of the ML-MoS_2 by dielectric screening and ground state charge transfer, as a function of Φ_{sub} and ε_r of the supporting substrate. Based on the measured parameters, we propose an empirical model, an extended Schottky-Mott rule, that enables predicting SBH values for ML-MoS_2 on any substrate, as long as no E_F-pinning-induced ground state charge transfer occurs between ML-MoS_2 and the substrate. This modified Schottky-Mott rule should be applicable to all 2D semiconductors if pertinent benchmark data for these become available.

RESULTS AND DISCUSSION

Substrate Work Function Dependent Schottky Barrier Height and Fermi Level Pinning. First, to investigate the correlation between SBH and Φ_{sub}, ML-MoS_2 samples were prepared on supporting substrates with Φ_{sub} in

https://doi.org/10.1021/acsnano.1c04825
ACS Nano 2021, 15, 14794−14803

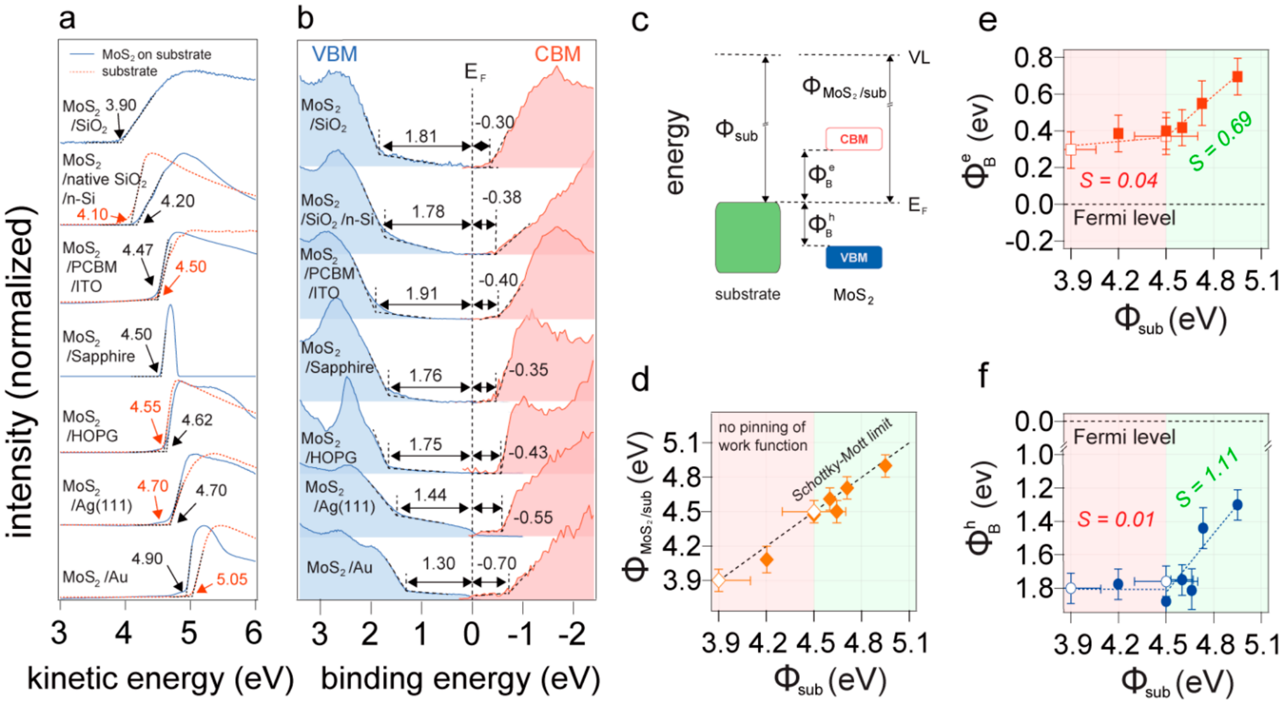

Figure 2. Substrate work function dependency of hole and electron barrier height ($\Phi_B{}^h$ and $\Phi_B{}^e$), and monolayer (ML)-MoS_2/substrate work function. (a) Secondary electron cutoff (SECO) spectra of ML-MoS_2 (blue solid lines) on top of polycrystalline Au, Ag(111), highly oriented pyrolytic graphite (HOPG), sapphire, phenyl-C61-butyric acid methyl ester (PCBM)/indium−tin-oxide (ITO), SiO_2 (native oxide)/*n*-Si and SiO_2 (thermal oxide) substrates. Dashed red lines correspond to the SECO spectra of the pristine substrates. (b) Valence (blue) and conduction (red) band spectra of ML-MoS_2 on top of supporting substrates at the K-point of the MoS_2 Brillouin zone. (c) Schematic diagram of energy level alignment between substrate and ML-MoS_2. (d) Work function values of ML-MoS_2/substrate ($\Phi_{MoS2/sub}$), (e) electron barrier ($\Phi_B{}^e$), and (f) hole barrier ($\Phi_B{}^h$) height of ML-MoS_2 plotted as a function of the substrate work function (Φ_{sub}). The measurement of Φ_{sub} for insulating substrates (sapphire and SiO_2-thermal oxide) is not possible (unfilled markers), the corresponding values are estimated and dressed with appropriately larger error bars, as further addressed in the SI.

the range of 4.2−5.05 eV. All sample preparation and measurement procedures are detailed in the Supporting Information (SI). ARIPES measurements were performed in order to determine $\Phi_B{}^e$ and ARPES measurements for $\Phi_B{}^h$, Φ_{sub} and $\Phi_{MoS2/sub}$, the latter being the sample work function of the ML-MoS_2 on the substrate. The ML-MoS_2 were grown by chemical vapor deposition (CVD) on sacrificial substrates, from which they were transferred onto each supporting substrate to avoid damage of ML-MoS_2 during an eventual metal evaporation step, as Duan et al. suggested.[29] Prior to ARPES and ARIPES measurements, the quality of transferred ML-MoS_2 was examined using optical microscopy, atomic force microscopy, reflectance, and photoluminescence measurements as shown in the SI Figure 1. The properties of the supporting substrates used in this study are summarized in SI Table S1.

Because Φ_{sub} is very sensitive to the surface properties, the supporting substrates were consistently prepared under the same conditions, such as exposure time to air and surface cleaning procedure, immediately before ML-MoS_2 transfer. The secondary cutoff (SECO) spectra of the ML-MoS_2/substrate samples and their supporting substrates are shown in Figure 2a as blue solid and red dashed lines, respectively. Since the SECO directly corresponds with the minimum energy needed to remove inelastically scattered electrons from the surface, it carries no information on the underlying pristine substrate, particularly as our ML-MoS_2 surface coverage is very high so that a few% uncovered substrate area is negligible.[44] From these spectra, the work function values of the ML-MoS_2/substrate ($\Phi_{MoS2/sub}$) samples and the bare supporting substrate (Φ_{sub}) were obtained and plotted in Figure 2d. In contrast to common belief,[24,25,27,28] $\Phi_{MoS2/sub}$ scales linearly with Φ_{sub} with a slope of almost one, which could indicate the absence of E_F-pinning. This observation is consistent with the recent SBH estimations reported by Duan et al.,[29,30] and supports their claim that damage by electrode deposition onto a TMDC results in strong E_F-pinning, at least from the work function perspective.

To directly assess Φ_B^e and Φ_B^h, ARPES and ARIPES were performed at the K-point of the ML-MoS_2 Brillouin zone (BZ), which yield the global VBM and CBM values, respectively (see SI Figure S3).[40,45] Because the photoemission signal of some substrates (particularly Au and Ag) is comparably strong and that of others is weak [sapphire and highly oriented pyrolytic graphite (HOPG)], the valence band spectra take on different overall appearances despite the predominant contribution from ML-MoS_2. Nonetheless, its pronounced VBM features at the K point of the BZ are clearly observable, which allows obtaining the binding energy of the VBM (onset of emission) with respect to the Fermi level. In analogy, the binding energy of the CBM with respect to the Fermi level was systematically extracted. All these values, corresponding to Φ_B^e and Φ_B^h, are plotted as a function of Φ_{sub} in Figure 2e,f.

If the Schottky−Mott rule applies, Φ_{sub} alone determines Φ_B^e and Φ_B^h, if IE and EA are constants, as depicted in Figure 2c. From this perspective, the correlation between $\Phi_{MoS2/sub}$ and Φ_{sub} in Figure 2d appears reasonable. In contrast, the plots of

https://doi.org/10.1021/acsnano.1c04825
ACS Nano 2021, 15, 14794−14803

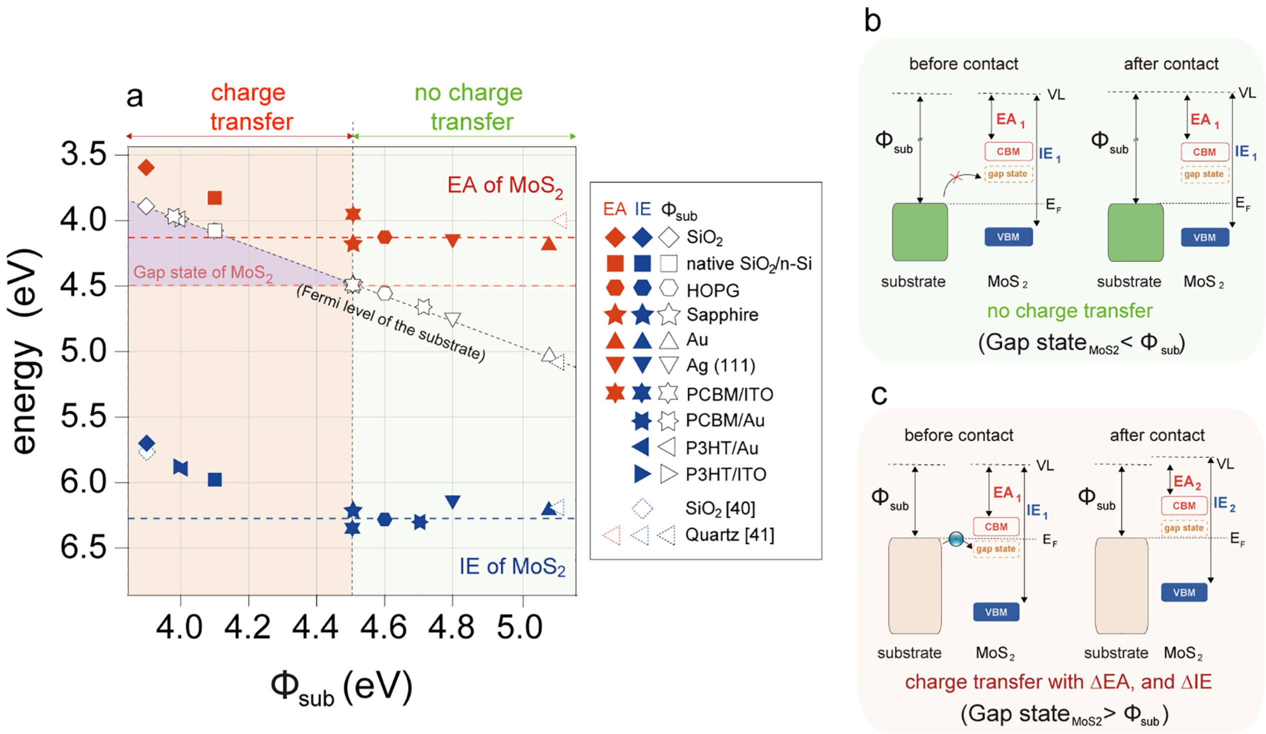

Figure 3. Energy levels of ML-MoS$_2$ as a function of substrate work function. (a) Plot of ionization energy (IE, blue) and electron affinity (EA, red) of ML-MoS$_2$ as a function of the bare substrate work function, for the substrates: polycrystalline Au, Ag(111), HOPG, sapphire, PCBM)/ITO, poly(3-hexylthiophene-2,5-diyl) (P3HT)/ITO, SiO$_2$ (native oxide)/*n*- Si, and SiO$_2$ (thermal oxide). The Fermi level positions of the bare supporting substrates with respect to the vacuum level are plotted as white symbols. Schematic energy diagrams before and after contact between ML-MoS$_2$ and a substrate, for the cases that before contact (b) gap state energy levels lie above the substrate Fermi level and (c) below the substrate Fermi level.

Figure 2e,f can be divided into two regions, bordering at Φ_{sub} of 4.5 eV. In the right-hand region (Φ_{sub} > 4.5 eV; shaded green), decreasing Φ_B^h and increasing Φ_B^e can be clearly observed with increasing Φ_{sub}. This seems at first glance to support the validity of the Schottky-Mott rule for ML-MoS$_2$/substrate. Upon closer inspection, the slope parameters *S* are fitted to be 1.11 for Φ_B^h and 0.69 for Φ_B^e. Notably, *S* for the electron barrier is significantly lower than 1, and for the electron barrier even a little higher than the ideal value of 1 of the Schottky−Mott rule. This asymmetry in the trends of hole and electron barriers as a function of Φ_{sub} has not been reported to date. This finding already implies that at least one factor is missing to establish a rule for the energy level alignment at ML-MoS$_2$/substrate interfaces.

In the second region (Φ_{sub} < 4.5 eV; shaded red), the charge injection barriers are pinned, at ca. 0.4 eV for electrons and ca. 1.80 eV for holes, with S ≈ 0 within the margin of experimental error. This is a clear indication of E$_F$-pinning, involving electron transfer from the substrate to the ML-MoS$_2$. For defect-free semiconductors these electrons are received by the conduction band. It was also suggested that gap states due to atomic defects in TMDCs are involved to establish the electronic balance at the charge neutrality level.[24] In this E_F-pinning study with various metals a value of 4.48 eV was derived for the charge neutrality level of MoS$_2$, which is very close to the work function value that we find here to dissect the region of essentially vacuum level alignment and E$_F$-pinning, i.e., 4.5 eV. Therefore, it is possible that charge transfer to defect levels in the gap of MoS$_2$ also plays a role here, and these have been suggested to have rather wide energy distribution below the conduction band.[46] The ground state electron transfer should result in a work function change (compared to Φ_{sub}) that is proportional to the amount of transferred charge.[47] However, as seen from Figure 2d, the observed difference between Φ_{sub} and $\Phi_{MoS2/sub}$ in the E_F-pinning region is too small (<0.2 eV) to be consistent with a constant IE and EA of ML-MoS$_2$ over the entire range of substrates investigated.

Variation of IE and EA of ML-MoS$_2$ due to ground state charge transfer. To elucidate the reason for the apparent variation of the IE and EA of ML-MoS$_2$ just mentioned above, we summarize the measured IE and EA values as a function of Φ_{sub}, including the values from previous reports,[48,49] in Figure 3a. The spectra and the corresponding determination of IE are detailed in SI Figure S4. The blue, red, and white symbols represent the IE and EA of ML-MoS$_2$, and Φ_{sub}, respectively. In the green shaded region of Figure 3a (Φ_{sub} > 4.5 eV), the IE and EA values of ML-MoS$_2$ exhibit a comparably small variation. The substrate E$_F$ is well within the band gap of ML-MoS$_2$ in this region, making electron transfer from the substrate to ML-MoS$_2$ unlikely, as illustrated in Figure 3b. In contrast, the red region of Figure 3a (Φ_{sub} < 4.5 eV) shows a decrease in IE and EA with decreasing Φ_{sub}. In this region, the energy position of E_F before contact (corresponding to Φ_{sub}) is lower than the native sulfur vacancy induced gap state of ML-MoS$_2$ (pink dashed line), which was reported at about 0.4 eV[27,28,50] below the conduction band minimum, corresponding to the EA of a pristine and charge-neutral ML-MoS$_2$. Notably, the energy of this gap state is then at ca. 4.5 eV below the vacuum level in Figure 2a, corresponding to the crossover work function value between the red and green areas. Because no charge transfer is expected

https://doi.org/10.1021/acsnano.1c04825
ACS Nano 2021, 15, 14794−14803

in in the green (unpinned) region, it is reasonable to assume that the measured IE and EA in the green region can be considered as intrinsic values for ML-MoS_2. In the red-shaded region of Figure 3a, the before-contact energy level alignment is favorable for electron transfer from the substrate to ML-MoS_2, as illustrated in Figure 3c. In fact, strong indication for excess electrons in experiments with ML-MoS_2 on SiO_2 as supporting substrate has been reported by the observations of enhanced trion photoluminescence,[51,52] in line with our suggestion that electron transfer occurs from the supporting substrate to ML-MoS_2 in the E_F-pinning region. This is also in line with a decrease in IE due to increased carrier screening.[53−56] While an increase in EA would be concomitantly expected due to band gap renormalization by doping, it is apparently not observed here. This is at odds with the simple picture of electron transfer to gap states, but could possibly be due to partial filling[57] and electron correlation induced splitting[58] of the conduction band by transferred electrons, so that the measured EA does no longer correspond to the conduction band minimum. To understand this in detail, further systematic doping experiments would be needed, which yet goes beyond the scope of this work.

Therefore, our observations underpin that, unlike in 3D systems, ground state charge transfer with a substrate can significantly renormalize the electronic structure and alter the IE and EA of 2D materials. From an application point of view, it is important to stress that IE and EA, which are often thought to be intrinsic properties of a material, are not constant, but depend on Φ_{sub} if charge transfer occurs. This can also provide a consistent explanation as why many previous studies have reported a wide range of IE values for ML-MoS_2 (5.7−6.2 eV) that extend far beyond the experimental error.[14,40,48,59−64]

Schottky-Mott Rule Expanded by Band Gap Renormalization. We now address the impact of dielectric screening by the substrate, which has been considered in discussion of the SBH so far. For this, E_g, IE, and EA of ML-MoS_2 are plotted as a function of the static dielectric constant of the supporting substrate (ε_r) as shown in Figure 4. Only supporting substrates with Φ_{sub} > 4.5 eV are used for this analysis, in order to exclude charge transfer induced changes in IE and EA due to E_F-pinning, as discussed in the previous section. From Figure 4 we observe the significant decrease of IE, increase of EA, and decrease of E_g (E_g = IE − EA) of the ML-MoS_2 with increasing substrate ε_r. Our present data are thus consistent with previous theoretical predictions by first-principles calculations using the GW approximation and further experimental data from scanning tunneling microscopy measurements.[36,65]

The origin of the E_g renormalization due to screening is the Coulomb interaction between confined holes/electrons inside the 2D monolayer and the surrounding dielectric medium,[54,66] and we can safely hypothesize that the change in E_g of ML-MoS_2 monolayer is thus governed by the Coulomb potential that is proportional to $1/\varepsilon_r$. Based on this, E_g of ML-MoS_2 as a function of ε_r of the substrate can be empirically expressed as

$$E_g(\varepsilon_r) = E_{g,\infty} + \alpha/\varepsilon_r \tag{1}$$

where $E_{g,\infty}$ is the single-particle band gap of ML-MoS_2 on a substrate with infinite ε_r, and α is an empirical constant (of the dimension energy) that includes information about the polarizability of the combined system. For ML-MoS_2, α =

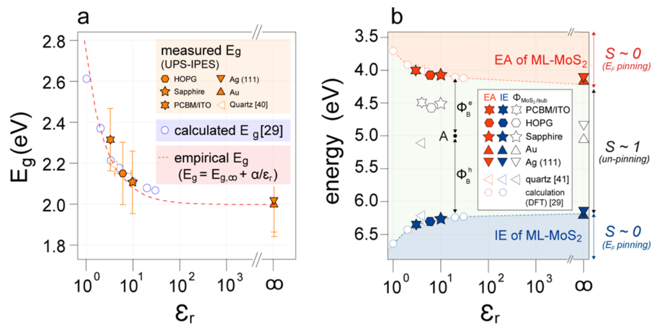

Figure 4. Energy levels of monolayer (ML)-MoS_2 as a function of substrate dielectric constant. (a) The single-particle band gap (E_g) of ML-MoS_2 plotted as a function of substrate static dielectric constant. The E_g were obtained from combined ARPES and ARIPES measurements. Reported E_g values from scanning tunneling spectroscopy and DFT calculations are plotted as blue circles and dashed triangle, respectively.[36,49] Details about the empirically estimated E_g (dashed line) are given in the main text. (b) Plot of ionization energy (IE), electron affinity (EA) and work function of ML-MoS_2 ($\Phi_{MoS2/sub}$) on different substrates, as a function of the substrate dielectric constant. The calculated IE, EA, and E_g values[36] of ML-MoS_2 are rigidly shifted to align with the measured values. Only supporting substrates with Φ_{sub} > 4.5 eV are plotted to rule ground state charge transfer effects (E_F-pinning).

0.9 eV and $E_{g,\infty}$ = 2.0 eV were obtained by fitting the experimental data in Figure 4a. Following the variation of E_g given by eq 1, the dependence of IE and EA with respect to ε_r can be written in the following way, assuming no difference of α for electrons and holes:

$$\mathrm{IE}(\varepsilon_r) = \mathrm{IE}_\infty + \alpha/2\varepsilon_r,\quad \mathrm{EA}(\varepsilon_r) = \mathrm{EA}_\infty - \alpha/2\varepsilon_r \tag{2}$$

where IE_∞ and EA_∞ are the ionization energy and electron affinity of a ML-MoS_2 on a substrate with infinite ε_r. Once IE_∞ and EA_∞ are determined by fitting experimental data with this equation, the SBH for electrons (holes) can be obtained by the energy difference between Φ_{sub} and EA (IE). For instance, mark A in Figure 4b represents an assumed supporting substrate having Φ_{sub} of 5 eV and ε_r of 20, and the specific SBH values, Φ_B^e and Φ_B^h, can be directly read from the graph, or computed by

$$\begin{aligned}\Phi_B^h(\Phi_{sub}, \varepsilon_r) &= \mathrm{IE}_\infty + \alpha/2\varepsilon_r - \Phi_{sub}\\ \Phi_B^e(\Phi_{sub}, \varepsilon_r) &= \Phi_{sub} - (\mathrm{EA}_\infty - \alpha/2\varepsilon_r)\end{aligned} \tag{3}$$

Using these equations, reasonably predicted Φ_B^h and Φ_B^e values, based on the parameters fitted from our data and the values of Φ_{sub} and ε_r, are obtained and itemized in Table 1.

The empirical parameter α in the expanded Schottky-Mott rule above (eq 3) is representative of the Coulomb interaction between individual confined in ML-MoS_2 and the surrounding dielectric. Therefore, the α used here is valid for ML-MoS_2. However, with appropriate experimental benchmark data, the proposed rule should be useful for estimating the SBH for other 2D semiconductors as well.

Asymmetry of the Pinning Parameter *S* for Electrons and Holes. With the expanded Schottky-Mott rule introduced above, we can now reconcile the observation made in Figure 2e,f that the pinning parameter *S* differs for electrons and holes, whereas they are expected to be the same in the original Schottky-Mott rule. As seen from Figure 5a, *S* gives the

Table 1. Predicted and Measured SBH and E_g Values[a]

	Φ_B^h		Φ_B^e		E_g	
substrate	measured	predicted	measured	predicted	measured	predicted
PCBM/ITO	1.91	1.84	0.40	0.38	2.31	2.23
HOPG	1.75	1.73	0.43	0.43	2.18	2.15
sapphire	1.76	1.74	0.35	0.34	2.11	2.08
Ag(111)	1.44	1.50	0.55	0.50	1.99	2.00
Au	1.30	1.30	0.70	0.70	2.00	2.00

[a]Comparison of measured and predicted Φ_B^h, Φ_B^e, and E_g values. The parameters used in the empirical model are IE_∞ = 6.2 eV, EA_∞ = 4.2 eV, $E_{g,\infty}$ = 2.0 eV, and α = 0.9 eV. All values are given in eV.

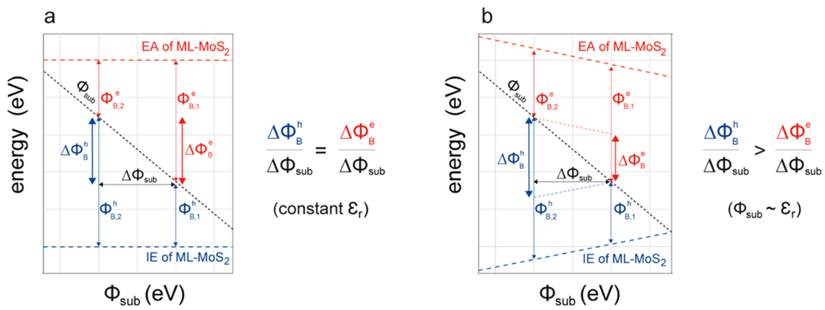

Figure 5. Origin of the asymmetric pinning parameters S for electrons and holes. The energy levels of ML-MoS$_2$ as a function of work function of the supporting substrate (Φ_{sub}), where the ionization energy (IE) and electron affinity (EA) is (a) constant and (b) vary with the dielectric constant of supporting substrate (ε_r), using the relations given in eq 3.

variation of Φ_B^h and Φ_B^e with Φ_{sub}, and both exhibit identical trends as long as IE and EA are constant. In our experiments, coincidentally, increasing Φ_{sub} goes in hand with increasing $\varepsilon_r(d\varepsilon_r/d\Phi_{sub} \neq 0)$ for our substrates. Therefore, as EA and IE change with ε_r, one can readily see that the S parameter becomes different from 1 and dependent on carrier type, as exemplified in Figure 5b. Using eq 3, the slope parameter for holes and electron can be calculated as

$$d\Phi_B^h/d\Phi_{sub} = |[d(^{\alpha}/_{2\varepsilon_r})/d\Phi_{sub}] - 1|$$

and

$$d\Phi_B^e/d\Phi_{sub} = |1 + [d(^{\alpha}/_{2\varepsilon_r})/d\Phi_{sub}]|$$

which returns different values. In our case, this yields S for holes of 1.11 (even higher than the ideal S of 1) and 0.69 for electrons. This emphasizes that Φ_{sub} and ε_r of the substrate must be considered simultaneously to appropriately determine the SBH and the interfacial energy level alignment.

Finally, an application point of view note regarding the TMDC energy levels further apart from the immediate electrode contact. In a lateral geometry, as found in monolayer-based field-effect transistors, the ML-TMDC rests on the gate dielectric next to the electrode. Since the (static) ε_r of the gate dielectric is lower than that of a metal, the band gap of the TMDC will increase as function of distance from the metal on the length scale of a few nm.[67] Accordingly, the injected charge carriers have to overcome an effective SBH that is larger (by approximately half the amount of the band gap renormalization) than the value immediately at the electrode contact. Accordingly, the effective SBH will be smaller when using modern high dielectric constant gate dielectrics. If the ML-TMDC is doped, additional band bending away from the electrode will occur, its magnitude depending on the doping level. The length-scale over which this band bending occurs has been explained in this geometry by the geometry-specific screening length by Appenzeller et al.,[68] and was estimated to be in the range of a few nm for typical material parameters, in accordance with an estimation from experiment.[67] We also note that the SBH derived from our model should be further adapted for bi- and multilayer TMDCs, as changes in band gap resulting from the different dielectric screening by the additional TMDC layer(s) will occur, alongside with a direct-to-indirect gap transition. Furthermore, the formation of space charge regions in the vertical direction is expected, which will result in a thickness-dependent SBH.[69]

CONCLUSIONS

From the present systematic study of the electronic energy levels at interfaces comprising ML-MoS$_2$ transferred onto a variety of substrates, including metals, semimetals, as well as organic and inorganic semiconductors and insulators, we infer how the charge injection barrier is impacted by the substrate work function Φ_{sub} and dielectric constant ε_r, simultaneously. Two different regimes of level alignment are observed: (i) for Φ_{sub} < 4.5 eV, strong Fermi level pinning occurs with $S \approx 0$. (ii) For Φ_{sub} > 4.5 eV, essentially vacuum level alignment takes place but the S values are different for electrons and holes. In the E_F-pinning regime (i), a significant reduction of the IE and EA of the ML-MoS$_2$ is observed and is attributed to pronounced band gap renormalization by electron transfer from the supporting substrate to the ML-MoS$_2$ gap states. In regime (ii) where no interfacial ground state charge transfer occurs, the Schottky barrier height depends on Φ_{sub} and the magnitude of dielectric screening by the supporting substrate. Because the dielectric screening induces band gap renormalization in 2D semiconductors, the slope parameter S can deviate from 1, even when vacuum level alignment prevails. For ML-MoS$_2$ this effect leads to asymmetric S values for electrons ($\approx$0.69) and holes ($\approx$1.11), the latter even exceeding the limit of 1 in the traditional Schottky-Mott rule. From this insight, we propose an empirical expansion of the Schottky-Mott rule to

https://doi.org/10.1021/acsnano.1c04825
ACS Nano 2021, 15, 14794−14803

account for the specific effects of the substrate's ε_r. This enables accurate predictions of the Schottky barrier height for ML-MoS_2 on virtually any supporting substrate. We propose that the expression for the expanded Schottky-Mott rule should be applicable to any 2D semiconductor monolayer, provided that appropriate benchmark data are available. The presented comprehensive picture of energy level alignment mechanisms enhances the reliability of interface design and electrical contact optimization for applications relying on 2D semiconductors.

METHODS

Sample Preparation. MoS_2 monolayers were grown on the substrates *via* chemical vapor deposition (CVD)[70] and transferred onto preprepared target supporting substrates using (1) the sonication method reported by Ma et al.[16] or (2) the thermal release tape method (TRT).[71] In brief, First, poly(methyl methacrylate) (PMMA, Micro Chem) layer was spin-coated onto the as-grown MoS_2 monolayer film and baked to form a stable scarified layer. (1) For sonication method, the PMMA/MoS_2 monolayer was sonicated for 1 min in a deionized water. After then, the PMMA/MoS_2 was peeled off and deposited on the Au, Ag (111), SiO_2, *n*-Si and HOPG. The fabricated structure of PMMA/MoS_2/substrates was baked for 1 h at 120 °C. (2) For TRT method, the TRT was attached on the PMMA/MoS_2 monolayer. After then, TRT/PMMA/MoS_2 monolayer was mechanically peeled from the as-grown MoS_2 monolayer film. After the separated TRT/PMMA/MoS_2 was transferred onto prespin coated P3HT (PCBM)/ITO substrate, the TRT was released from the sample by heating on a hot plate at 110 °C for 2 min. Finally, for both cases, the top PMMA layer was removed by using the acetone. To ensure the possible damage of relative weak organic layer (P3HT and PCBM), pristine Poly(3-hexylthiophene-2,5-diyl) (P3HT) and [6,6]-Phenyl C61 butyric acid methyl ester (PCBM) on ITO that were dipped in the acetone for 20 min and it were tested using ARPES and optical microscopy, which are proven to no change.

ARPES and ARIPES Measurements. Prior to the ARPES and ARIPES measurements, all MoS_2 monolayer samples were annealed overnight at 300−350 °C *in situ* in an ultrahigh vacuum (UHV) preparation chamber (10^{-9} mbar) to remove carbon contamination and residual poly(methyl methacrylate) involved during the transfer process. Valence band spectra were obtained using a hemispherical electron analyzer (Phoibos-100 and SCIENTA DA30) with standard He I_α (21.22 eV) discharge lamp. To obtain the accurate VBM onset, the contribution from the He I_β satellite was removed in all PES spectra presented in this study. External bias of −10 V is applied to the sample to measure the reliable secondary electron cutoff (SECO) spectra. Conduction band spectra were obtained using the isochromat mode photodetector consisting a BaO cathode and a band-pass filter of 9.5 eV (SrF_2 + NaCl) with a low-energy electron gun. The energy reference of both instruments was calibrated by measuring the Fermi edge of clean Au (111) sample. The instrumental energy resolution was of 0.14 and 0.30 eV for ARPES and ARIPES, respectively. Deconvolution procedure were carried out for IPES spectra to obtain the more accurate onset of CBM, and the details are in previous studies.[40]

Optical Measurement. Reflectance measurements were either performed using a microscope setup (samples on *n*-Si, SiO_2/Si, and HOPG) or using an integrating sphere (samples on Au and sapphire). White light from a tungsten halogen lamp was used. The differential reflectance (DR) spectra, defined as DR = $(R - R_0)/R_0$ were used to obtain exciton transition energies on the opaque substrates. Here, R is the reflectance from MoS_2 monolayer on the substrate and R_0 is the reflectance from the substrate only. For MoS_2 monolayer on sapphire and Au, the DR spectra were multiplied with (−1) for clarity. In order to extract the positions of the A and B exciton and compare them to literature, the DR spectra on SiO_2/Si and HOPG were modeled with a Lorentz oscillator model and fitted with a transfer matrix method using the dielectric functions of the substrates from literature. Absorbance (samples on ITO) was measured using a PerkinElmer Lambda 950 UV−vis-NIR spectrometer. PL spectra were obtained in a microscope PL setup exciting with a laser diode at 2.82 eV. The emission was dispersed in an Acton SpectraPro 2500i spectrograph equipped with a liquid nitrogen cooled CCD (Acton SPEC-10:100).

ASSOCIATED CONTENT

Supporting Information

The Supporting Information is available free of charge at https://pubs.acs.org/doi/10.1021/acsnano.1c04825.

Optical microscopy images; Differential reflectance/absorption spectroscopy; Photoluminescence spectroscopy; Information on supporting substrates; Atomic force microscopy images of the supporting substrates; Calculated band structure of ML-MoS_2; Angle-resolved photoemission spectroscopy of ML-MoS_2 (PDF)

AUTHOR INFORMATION

Corresponding Authors

Soohyung Park − *Advanced Analysis Center, Korea Institute of Science and Technology (KIST), Seoul 02792, South Korea;* orcid.org/0000-0002-6589-7045; Email: soohyung.park@kist.re.kr

Norbert Koch − *Humboldt-Universität zu Berlin, Institut für Physik & IRIS Adlershof, 12489 Berlin, Germany; Helmholtz-Zentrum für Materialien und Energie GmbH, Bereich Solarenergieforschung, 12489 Berlin, Germany;* orcid.org/0000-0002-6042-6447; Email: norbert.koch@physik.hu-berlin.de

Authors

Thorsten Schultz − *Humboldt-Universität zu Berlin, Institut für Physik & IRIS Adlershof, 12489 Berlin, Germany; Helmholtz-Zentrum für Materialien und Energie GmbH, Bereich Solarenergieforschung, 12489 Berlin, Germany;* orcid.org/0000-0002-0344-6302

Dongguen Shin − *Humboldt-Universität zu Berlin, Institut für Physik & IRIS Adlershof, 12489 Berlin, Germany*

Niklas Mutz − *Humboldt-Universität zu Berlin, Institut für Physik & IRIS Adlershof and Institut für Chemie, 12489 Berlin, Germany;* orcid.org/0000-0002-0018-6445

Areej Aljarb − *Physical Sciences and Engineering, King Abdullah University of Science and Technology, Thuwal 23955-6900, Saudi Arabia; Department of Physics, King Abdulaziz University, Jeddah 21589, Kingdom of Saudi Arabia*

Hee Seong Kang − *KU-KIST Graduate School of Converging Science and Technology & Department of Integrative Energy Engineering, Korea University, Seoul 02841, Republic of Korea; Advanced Materials Research Division, Korea Institute of Science and Technology, Seoul 02792, Republic of Korea*

Chul-Ho Lee − *KU-KIST Graduate School of Converging Science and Technology & Department of Integrative Energy Engineering, Korea University, Seoul 02841, Republic of Korea; Advanced Materials Research Division, Korea Institute of Science and Technology, Seoul 02792, Republic of Korea;* orcid.org/0000-0003-1570-8688

Lain-Jong Li − *Department of Mechanical Engineering, The University of Hong Kong, Hong Kong*

Xiaomin Xu − *Tsinghua-Berkeley Shenzhen Institute & Tsinghua Shenzhen International Graduate School, Tsinghua University, Shenzhen 518055, China*

Vincent Tung − *Physical Sciences and Engineering, King Abdullah University of Science and Technology, Thuwal 23955-6900, Saudi Arabia*

Emil J. W. List-Kratochvil − *Humboldt-Universität zu Berlin, Institut für Physik & IRIS Adlershof and Institut für Chemie, 12489 Berlin, Germany; Helmholtz-Zentrum für Materialien und Energie GmbH, Bereich Solarenergieforschung, 12489 Berlin, Germany;* orcid.org/0000-0001-9206-800X

Sylke Blumstengel − *Humboldt-Universität zu Berlin, Institut für Physik & IRIS Adlershof and Institut für Chemie, 12489 Berlin, Germany*

Patrick Amsalem − *Humboldt-Universität zu Berlin, Institut für Physik & IRIS Adlershof, 12489 Berlin, Germany;* orcid.org/0000-0002-7330-2451

Complete contact information is available at: https://pubs.acs.org/10.1021/acsnano.1c04825

Author Contributions

S.P., T.S., S.B., X.X., D.S., and P.A. performed ARPES and ARIPES measurements, and analyzed all data, under supervision of N.K.. N.M., and S.B. performed optical measurements to ensure sample quality. S.P., T.S., S.B., X.X., D.S., P.A., and N.K. wrote the manuscript. D.S., T.S., and P.A. revised the manuscript. A.A., A.H., H.S.K., C.L., and V.T. prepared the ML-MoS_2 samples. All authors commented on the manuscript.

Notes

The authors declare no competing financial interest.

ACKNOWLEDGMENTS

This work was funded by the Deutsche Forschungsgemeinschaft (DFG, German Research Foundation) Project No. 182087777 - SFB 951. Further support by the National Research Foundation (NRF) of Korea under Grant 2018M3D1A1058793 and Technology Innovation Program (20012502), funded by the Korean Ministry of Trade, Industry & Energy, is acknowledged. This work was supported by the KIST Institutional Program (Project No. 2 V09108). C.-H. Lee acknowledges the support from the KU-KIST School Project. V.T. and A.A. are indebted to the support from the King Abdullah University of Science and Technology (KAUST) Office of Sponsored Research (OSR) under award no. OSR-2018-CARF/CCF-3079.

REFERENCES

(1) Chhowalla, M.; Shin, H. S.; Eda, G.; Li, L.-J.; Loh, K. P.; Zhang, H. The Chemistry of Two-Dimensional Layered Transition Metal Dichalcogenide Nanosheets. *Nat. Chem.* **2013**, *5* (4), 263−275.

(2) McDonnell, S. J.; Wallace, R. M. Atomically-Thin Layered Films for Device Applications Based upon 2D TMDC Materials. *Thin Solid Films* **2016**, *616*, 482−501.

(3) Wang, Q. H.; Kalantar-Zadeh, K.; Kis, A.; Coleman, J. N.; Strano, M. S. Electronics and Optoelectronics of Two-Dimensional Transition Metal Dichalcogenides. *Nat. Nanotechnol.* **2012**, *7* (11), 699−712.

(4) Ye, M.; Winslow, D.; Zhang, D.; Pandey, R.; Yap, Y. Recent Advancement on the Optical Properties of Two-Dimensional Molybdenum Disulfide (MoS_2) Thin Films. *Photonics* **2015**, *2* (1), 288−307.

(5) Li, H.; Shi, Y.; Chiu, M. H.; Li, L. J. Emerging Energy Applications of Two-Dimensional Layered Transition Metal Dichalcogenides. *Nano Energy* **2015**, *18*, 293−305.

(6) Chhowalla, M.; Jena, D.; Zhang, H. Two-Dimensional Semiconductors for Transistors. *Nat. Rev. Mater.* **2016**, *1* (11), 16052.

(7) Fiori, G.; Bonaccorso, F.; Iannaccone, G.; Palacios, T.; Neumaier, D.; Seabaugh, A.; Banerjee, S. K.; Colombo, L. Electronics Based on Two-Dimensional Materials. *Nat. Nanotechnol.* **2014**, *9* (10), 768−779.

(8) Radisavljevic, B.; Radenovic, A.; Brivio, J.; Giacometti, V.; Kis, A.; Radisavljevic, B.; Radenovic, A.; Brivio, J.; Giacometti, V.; Kis, A. Single-Layer MoS_2 Transistors. *Nat. Nanotechnol.* **2011**, *6* (3), 147−150.

(9) Wang, H.; Yu, L.; Lee, Y.-H.; Shi, Y.; Hsu, A.; Chin, M. L.; Li, L.-J.; Dubey, M.; Kong, J.; Palacios, T. Integrated Circuits Based on Bilayer MoS_2 Transistors. *Nano Lett.* **2012**, *12* (9), 4674−4680.

(10) Sarkar, D.; Liu, W.; Xie, X.; Anselmo, A. C.; Mitragotri, S.; Banerjee, K. MoS_2 Field-Effect Transistor for Next-Generation Label-Free Biosensors. *ACS Nano* **2014**, *8* (4), 3992−4003.

(11) Sebastian, A.; Pendurthi, R.; Choudhury, T. H.; Redwing, J. M.; Das, S. Benchmarking Monolayer MoS_2 and WS_2 Field-Effect Transistors. *Nat. Commun.* **2021**, *12* (1), 693.

(12) Utama, M. I. B.; Kleemann, H.; Zhao, W.; Ong, C. S.; da Jornada, F. H.; Qiu, D. Y.; Cai, H.; Li, H.; Kou, R.; Zhao, S.; Wang, S.; Watanabe, K.; Taniguchi, T.; Tongay, S.; Zettl, A.; Louie, S. G.; Wang, F. A Dielectric-Defined Lateral Heterojunction in a Monolayer Semiconductor. *Nat. Electron.* **2019**, *2* (2), 60−65.

(13) Bernardi, M.; Palummo, M.; Grossman, J. C. Extraordinary Sunlight Absorption and One Nanometer Thick Photovoltaics Using Two-Dimensional Monolayer Materials. *Nano Lett.* **2013**, *13* (8), 3664−3670.

(14) Tsai, M.-L.; Su, S.-H.; Chang, J.-K.; Tsai, D.-S.; Chen, C.-H.; Wu, C.-I.; Li, L.-J.; Chen, L.-J.; He, J.-H. Monolayer MoS_2 Heterojunction Solar Cells. *ACS Nano* **2014**, *8* (8), 8317−8322.

(15) Huang, Y.; Zhuge, F.; Hou, J.; Lv, L.; Luo, P.; Zhou, N.; Gan, L.; Zhai, T. Van Der Waals Coupled Organic Molecules with Monolayer MoS_2 for Fast Response Photodetectors with Gate-Tunable Responsivity. *ACS Nano* **2018**, *12* (4), 4062−4073.

(16) Ma, D.; Shi, J.; Ji, Q.; Chen, K.; Yin, J.; Lin, Y.; Zhang, Y.; Liu, M.; Feng, Q.; Song, X.; Guo, X.; Zhang, J.; Zhang, Y.; Liu, Z. A Universal Etching-Free Transfer of MoS_2 Films for Applications in Photodetectors. *Nano Res.* **2015**, *8* (11), 3662−3672.

(17) Jayachandran, D.; Oberoi, A.; Sebastian, A.; Choudhury, T. H.; Shankar, B.; Redwing, J. M.; Das, S. A Low-Power Biomimetic Collision Detector Based on an In-Memory Molybdenum Disulfide Photodetector. *Nat. Electron.* **2020**, *3* (10), 646−655.

(18) Shen, P.-C.; Su, C.; Lin, Y.; Chou, A.-S.; Cheng, C.-C.; Park, J.-H.; Chiu, M.-H.; Lu, A.-Y.; Tang, H.-L.; Tavakoli, M. M.; Pitner, G.; Ji, X.; Cai, Z.; Mao, N.; Wang, J.; Tung, V.; Li, J.; Bokor, J.; Zettl, A.; Wu, C.-I.; Palacios, T.; Li, L.-J.; Kong, J. Ultralow Contact Resistance between Semimetal and Monolayer Semiconductors. *Nature* **2021**, *593* (7858), 211−217.

(19) Schottky, W. Halbleitertheorie Der Sperrschicht. *Naturwissenschaften* **1938**, *26* (52), 843−843.

(20) Mott, N. F. *Theory of Crystal Rectifiers* **1995**, *1*, 153−165.

(21) Tung, R. T. The Physics and Chemistry of the Schottky Barrier Height. *Appl. Phys. Rev.* **2014**, *1* (1), 011304.

(22) Yu, P. Y.; Cardona, M. *Fundamentals of Semiconductors*; 4th ed.; Graduate Texts in Physics; Springer Berlin Heidelberg: Berlin, Heidelberg, 2010.

(23) Das, S.; Chen, H.-Y.; Penumatcha, A. V.; Appenzeller, J. High Performance Multilayer MoS_2 Transistors with Scandium Contacts. *Nano Lett.* **2013**, *13* (1), 100−105.

(24) Kim, C.; Moon, I.; Lee, D.; Choi, M. S.; Ahmed, F.; Nam, S.; Cho, Y.; Shin, H.-J. J.; Park, S.; Yoo, W. J. Fermi Level Pinning at Electrical Metal Contacts of Monolayer Molybdenum Dichalcogenides. *ACS Nano* **2017**, *11* (2), 1588−1596.

(25) Kim, G.-S.; Kim, S.-H.; Park, J.; Han, K. H.; Kim, J.; Yu, H.-Y. Schottky Barrier Height Engineering for Electrical Contacts of Multilayered MoS_2 Transistors with Reduction of Metal-Induced Gap States. *ACS Nano* **2018**, *12* (6), 6292−6300.

(26) Bampoulis, P.; van Bremen, R.; Yao, Q.; Poelsema, B.; Zandvliet, H. J. W.; Sotthewes, K. Defect Dominated Charge

Transport and Fermi Level Pinning in MoS_2/Metal Contacts. *ACS Appl. Mater. Interfaces* **2017**, *9* (22), 19278−19286.

(27) Liu, D.; Guo, Y.; Fang, L.; Robertson, J. Sulfur Vacancies in Monolayer MoS_2 and Its Electrical Contacts. *Appl. Phys. Lett.* **2013**, *103* (18), 183113.

(28) Guo, Y.; Liu, D.; Robertson, J. Chalcogen Vacancies in Monolayer Transition Metal Dichalcogenides and Fermi Level Pinning at Contacts. *Appl. Phys. Lett.* **2015**, *106* (17), 173106.

(29) Liu, Y.; Guo, J.; Zhu, E.; Liao, L.; Lee, S.-J.; Ding, M.; Shakir, I.; Gambin, V.; Huang, Y.; Duan, X. Approaching the Schottky−Mott Limit in van der Waals Metal−Semiconductor Junctions. *Nature* **2018**, *557* (7707), 696−700.

(30) Went, C. M.; Wong, J.; Jahelka, P. R.; Kelzenberg, M.; Biswas, S.; Hunt, M. S.; Carbone, A.; Atwater, H. A. A New Metal Transfer Process for van der Waals Contacts to Vertical Schottky-Junction Transition Metal Dichalcogenide Photovoltaics. *Sci. Adv.* **2019**, *5* (12), No. eaax6061.

(31) Crowell, C. R. The Richardson Constant for Thermionic Emission in Schottky Barrier Diodes. *Solid-State Electron.* **1965**, *8* (4), 395−399.

(32) Heras, J. M.; Viscido, L. Work Function Changes upon Water Contamination of Metal Surfaces. *Appl. Surf. Sci.* **1980**, *4* (2), 238−241.

(33) Wan, A.; Hwang, J.; Amy, F.; Kahn, A. Impact of Electrode Contamination on the α-NPD/Au Hole Injection Barrier. *Org. Electron.* **2005**, *6* (1), 47−54.

(34) Turetta, N.; Sedona, F.; Liscio, A.; Sambi, M.; Samorì, P. Au(111) Surface Contamination in Ambient Conditions: Unravelling the Dynamics of the Work Function in Air. *Adv. Mater. Interfaces* **2021**, *8* (10), 2100068.

(35) Schulman, D. S.; Arnold, A. J.; Das, S. Contact Engineering for 2D Materials and Devices. *Chem. Soc. Rev.* **2018**, *47* (9), 3037−3058.

(36) Ryou, J.; Kim, Y.-S.; Kc, S.; Cho, K. Monolayer MoS_2 Bandgap Modulation by Dielectric Environments and Tunable Bandgap Transistors. *Sci. Rep.* **2016**, *6* (March), 29184.

(37) Kylänpää, I.; Komsa, H.-P. Binding Energies of Exciton Complexes in Transition Metal Dichalcogenide Monolayers and Effect of Dielectric Environment. *Phys. Rev. B: Condens. Matter Mater. Phys.* **2015**, *92* (20), 205418.

(38) Xiao, Y.; Li, Z.-Q.; Wang, Z.-W. Polaron Effect on the Bandgap Modulation in Monolayer Transition Metal Dichalcogenides. *J. Phys.: Condens. Matter* **2017**, *29* (48), 485001.

(39) Wang, Z. W.; Xiao, Y.; Li, R. Z.; Li, W. P.; Li, Z. Q. Self-Energy Effect and Coulomb Potential Modulation of the Exciton in Monolayer MoS_2 on Polar Substrate. *J. Phys. D: Appl. Phys.* **2017**, *50* (47).475306

(40) Park, S.; Mutz, N.; Schultz, T.; Blumstengel, S.; Han, A.; Aljarb, A.; Li, L.-J.; List-Kratochvil, E. J. W.; Amsalem, P.; Koch, N. Direct Determination of Monolayer MoS_2 and WSe_2 Exciton Binding Energies on Insulating and Metallic Substrates. *2D Mater.* **2018**, *5* (2), 025003.

(41) Lin, Y.; Ling, X.; Yu, L.; Huang, S.; Hsu, A. L.; Lee, Y.-H.; Kong, J.; Dresselhaus, M. S.; Palacios, T. Dielectric Screening of Excitons and Trions in Single-Layer MoS_2. *Nano Lett.* **2014**, *14* (10), 5569−5576.

(42) Wang, G.; Chernikov, A.; Glazov, M. M.; Heinz, T. F.; Marie, X.; Amand, T.; Urbaszek, B. Colloquium: Excitons in Atomically Thin Transition Metal Dichalcogenides. *Rev. Mod. Phys.* **2018**, *90* (2), 021001.

(43) Chernikov, A.; Berkelbach, T. C.; Hill, H. M.; Rigosi, A.; Li, Y.; Aslan, O. B.; Reichman, D. R.; Hybertsen, M. S.; Heinz, T. F. Exciton Binding Energy and Nonhydrogenic Rydberg Series in Monolayer WS_2. *Phys. Rev. Lett.* **2014**, *113* (7), 076802.

(44) Schultz, T.; Lenz, T.; Kotadiya, N.; Heimel, G.; Glasser, G.; Berger, R.; Blom, P. W. M.; Amsalem, P.; de Leeuw, D. M.; Koch, N. Reliable Work Function Determination of Multicomponent Surfaces and Interfaces: The Role of Electrostatic Potentials in Ultraviolet Photoelectron Spectroscopy. *Adv. Mater. Interfaces* **2017**, *1700324*, 1700324.

(45) Park, S.; Schultz, T.; Han, A.; Aljarb, A.; Xu, X.; Beyer, P.; Opitz, A.; Ovsyannikov, R.; Li, L.-J.; Meissner, M.; Yamaguchi, T.; Kera, S.; Amsalem, P.; Koch, N. Electronic Band Dispersion Determination in Azimuthally Disordered Transition-Metal Dichalcogenide Monolayers. *Commun. Phys.* **2019**, *2* (1), 68.

(46) Fang, N.; Nagashio, K. Band Tail Interface States and Quantum Capacitance in a Monolayer Molybdenum Disulfide Field-Effect-Transistor. *J. Phys. D: Appl. Phys.* **2018**, *51* (6), 065110.

(47) Oehzelt, M.; Koch, N.; Heimel, G. Organic Semiconductor Density of States Controls the Energy Level Alignment at Electrode Interfaces. *Nat. Commun.* **2014**, *5* (1), 4174.

(48) Keyshar, K.; Berg, M.; Zhang, X.; Vajtai, R.; Gupta, G.; Chan, C. K.; Beechem, T. E.; Ajayan, P. M.; Mohite, A. D.; Ohta, T. Experimental Determination of the Ionization Energies of $MoSe_2$, WS_2, and MoS_2 on SiO_2 Using Photoemission Electron Microscopy. *ACS Nano* **2017**, *11* (8), 8223−8230.

(49) Hill, H. M.; Rigosi, A. F.; Rim, K. T.; Flynn, G. W.; Heinz, T. F. Band Alignment in MoS_2/WS_2 Transition Metal Dichalcogenide Heterostructures Probed by Scanning Tunneling Microscopy and Spectroscopy. *Nano Lett.* **2016**, *16* (8), 4831−4837.

(50) Wang, D.; Li, X.-B.; Han, D.; Tian, W. Q.; Sun, H.-B. Engineering Two-Dimensional Electronics by Semiconductor Defects. *Nano Today* **2017**, *16* (October), 30−45.

(51) Mouri, S.; Miyauchi, Y.; Matsuda, K. Tunable Photoluminescence of Monolayer MoS_2*via* Chemical Doping. *Nano Lett.* **2013**, *13* (12), 5944−5948.

(52) Li, Y.; Qi, Z.; Liu, M.; Wang, Y.; Cheng, X.; Zhang, G.; Sheng, L. Photoluminescence of Monolayer MoS_2 on $LaAlO_3$ and $SrTiO_3$ Substrates. *Nanoscale* **2014**, *6* (24), 15248−15254.

(53) Qiu, Z.; Trushin, M.; Fang, H.; Verzhbitskiy, I.; Gao, S.; Laksono, E.; Yang, M.; Lyu, P.; Li, J.; Su, J.; Telychko, M.; Watanabe, K.; Taniguchi, T.; Wu, J.; Neto, A. H. C.; Yang, L.; Eda, G.; Adam, S.; Lu, J. Giant Gate-Tunable Bandgap Renormalization and Excitonic Effects in a 2D Semiconductor. *Sci. Adv.* **2019**, *5* (7).eaaw2347

(54) Liu, F.; Ziffer, M. E.; Hansen, K. R.; Wang, J.; Zhu, X. Direct Determination of Band-Gap Renormalization in the Photoexcited Monolayer MoS_2. *Phys. Rev. Lett.* **2019**, *122* (24), 246803.

(55) Liang, Y.; Yang, L. Carrier Plasmon Induced Nonlinear Band Gap Renormalization in Two-Dimensional Semiconductors. *Phys. Rev. Lett.* **2015**, *114* (6), 063001.

(56) Dolui, K.; Rungger, I.; Sanvito, S. Origin of the *n*-Type and *p*-Type Conductivity of MoS_2 Monolayers on a SiO_2 Substrate. *Phys. Rev. B: Condens. Matter Mater. Phys.* **2013**, *87* (16), 1−7.

(57) Caruso, F.; Amsalem, P.; Ma, J.; Aljarb, A.; Schultz, T.; Zacharias, M.; Tung, V.; Koch, N.; Draxl, C. Two-Dimensional Plasmonic Polarons in *n-Doped* Monolayer MoS_2. *Phys. Rev. B: Condens. Matter Mater. Phys.* **2021**. DOI: 10.1103/PhysRevB.103.205152

(58) van Loon, E. G. C. P.; Schüler, M.; Springer, D.; Sangiovanni, G.; Tomczak, J. M.; Wehling, T. O. Coulomb Engineering of Two-Dimensional Mott Materials. *arXiv* **2020**, No. 1, 1−9.

(59) Choudhury, P.; Ravavarapu, L.; Dekle, R.; Chowdhury, S. Modulating Electronic and Optical Properties of Monolayer MoS 2 Using Nonbonded Phthalocyanine Molecules. *J. Phys. Chem. C* **2017**, *121* (5), 2959−2967.

(60) Pierucci, D.; Henck, H.; Ben Aziza, Z.; Naylor, C. H.; Balan, A.; Rault, J. E.; Silly, M. G.; Dappe, Y. J.; Bertran, F.; Le Fèvre, P.; Sirotti, F.; Johnson, A. T. C.; Ouerghi, A. Tunable Doping in Hydrogenated Single Layered Molybdenum Disulfide. *ACS Nano* **2017**, *11* (2), 1755−1761.

(61) Lee, S. Y.; Kim, U. J.; Chung, J.; Nam, H.; Jeong, H. Y.; Han, G. H.; Kim, H.; Oh, H. M.; Lee, H.; Kim, H.; Roh, Y.-G.; Kim, J.; Hwang, S. W.; Park, Y.; Lee, Y. H. Large Work Function Modulation of Monolayer MoS_2 by Ambient Gases. *ACS Nano* **2016**, *10* (6), 6100−6107.

(62) Lin, J.; Zhong, J.; Zhong, S.; Li, H.; Zhang, H.; Chen, W. Modulating Electronic Transport Properties of MoS_2 Field Effect Transistor by Surface Overlayers. *Appl. Phys. Lett.* **2013**, *103* (6), 063109.

https://doi.org/10.1021/acsnano.1c04825
ACS Nano 2021, 15, 14794−14803

(63) Niklas, J.; Mardis, K. L.; Banks, B. P.; Grooms, G. M.; Sperlich, A.; Dyakonov, V.; Beaupré, S.; Leclerc, M.; Xu, T.; Yu, L.; Poluektov, O. G. Highly-Efficient Charge Separation and Polaron Delocalization in Polymer-Fullerene Bulk-Heterojunctions: A Comparative Multi-Frequency EPR and DFT Study. *Phys. Chem. Chem. Phys.* **2013**, *15* (24), 9562−9574.

(64) Park, S.; Schultz, T.; Xu, X.; Wegner, B.; Aljarb, A.; Han, A.; Li, L.; Tung, V. C.; Amsalem, P.; Koch, N. Demonstration of the Key Substrate-Dependent Charge Transfer Mechanisms between Monolayer MoS_2 and Molecular Dopants. *Commun. Phys.* **2019**, *2* (1), 109.

(65) Shi, J.; Liu, M.; Wen, J.; Ren, X.; Zhou, X.; Ji, Q.; Ma, D.; Zhang, Y.; Jin, C.; Chen, H.; Deng, S.; Xu, N.; Liu, Z.; Zhang, Y. All Chemical Vapor Deposition Synthesis and Intrinsic Bandgap Observation of MoS_2/Graphene Heterostructures. *Adv. Mater.* **2015**, *27* (44), 7086−7092.

(66) Waldecker, L.; Raja, A.; Rösner, M.; Steinke, C.; Bostwick, A.; Koch, R. J.; Jozwiak, C.; Taniguchi, T.; Watanabe, K.; Rotenberg, E.; Wehling, T. O.; Heinz, T. F. Rigid Band Shifts in Two-Dimensional Semiconductors through External Dielectric Screening. *Phys. Rev. Lett.* **2019**, *123* (20), 206403.

(67) Song, Z.; Schultz, T.; Ding, Z.; Lei, B.; Han, C.; Amsalem, P.; Lin, T.; Chi, D.; Wong, S. L.; Zheng, Y. J.; Li, M.-Y.; Li, L.-J.; Chen, W.; Koch, N.; Huang, Y. L.; Wee, A. T. S. Electronic Properties of a 1D Intrinsic/*p-Doped* Heterojunction in a 2D Transition Metal Dichalcogenide Semiconductor. *ACS Nano* **2017**, *11* (9), 9128−9135.

(68) Appenzeller, J.; Zhang, F.; Das, S.; Knoch, J. Transition Metal Dichalcogenide Schottky Barrier Transistors: A Device Analysis and Material Comparison. In *2D Materials for Nanoelectronics*; Houssa, M., Dimoulas, A., Molle, A., Eds.; CRC Press: Portland, 2016; pp 223−256.

(69) Wang, Q.; Shao, Y.; Gong, P.; Shi, X. Metal−2D Multilayered Semiconductor Junctions: Layer-Number Dependent Fermi-Level Pinning. *J. Mater. Chem. C* **2020**, *8* (9), 3113−3119.

(70) Li, M.-Y.; Shi, Y.; Cheng, C.-C.; Lu, L.-S.; Lin, Y.-C.; Tang, H.-L.; Tsai, M.-L.; Chu, C.-W.; Wei, K.-H.; He, J.-H.; Chang, W.-H.; Suenaga, K.; Li, L.-J. Epitaxial Growth of a Monolayer WSe_2-MoS_2 Lateral *p-n* Junction with an Atomically Sharp Interface. *Science* **2015**, *349* (6247), 524−528.

(71) Kang, K.; Xie, S.; Huang, L.; Han, Y.; Huang, P. Y.; Mak, K. F.; Kim, C.-J.; Muller, D.; Park, J. High-Mobility Three-Atom-Thick Semiconducting Films with Wafer-Scale Homogeneity. *Nature* **2015**, *520* (7549), 656−660.

https://doi.org/10.1021/acsnano.1c04825
ACS Nano 2021, 15, 14794−14803